http://ansinet.com/itj

ITJ

ISSN 1812-5638

INFORMATION TECHNOLOGY JOURNAL

ANSInet
Asian Network for Scientific Information
308 Lasani Town, Sargodha Road, Faisalabad - Pakistan

Information Technology Journal 12 (9): 1685-1695, 2013
ISSN 1812-5638 / DOI: 10.3923/itj.2013.1685.1695

Realization of Constant-Current Mode for a Contactless Battery Charging System

[1]Yan-Ling Li, [1]Zheng-You He, [2]Yue Sun and [2]Xin Dai
[1]Department of Electrical Engineering, Southwest Jiaotong University, China
[2]Department of Automation, Chongqing University, China

Abstract: For a contactless battery charging system based on inductively coupled power transfer technology, a generalized state-space averaging method is first introduced, which can convert the original system with the oscillating and nonlinear characteristics to a linear time-invariant system by using the low-order Fourier series to approximate the original circuit signals and nonlinear terms and then the performance weighting functions for multi-objective optimization are adjusted and chosen in the frequency domain to reflect the uncertainties of low frequency parameters and high frequency un-modeled part. To fulfill a robust stability and robust performance design in the constant-current mode, a H_∞ synthesis control algorithm solved by the linear matrix inequality method is proposed for the contactless battery charging system. All the results of computer simulation and practical experiment show that with the help of H_∞ control strategy, the system has successfully realized operating at the constant-current charging mode, dynamically tracking the current reference according to the battery charging requirements, rapidly inhibiting the adverse effects of battery voltage changes and load or frequency perturbations on the system. Therefore, the H_∞ control strategy used for contactless battery charging system is effective and practicable.

Key words: Constant-current, charging system, inductively coupled power transfer, robustness

INTRODUCTION

The contactless battery charging system is based on Inductively Coupled Power Transfer (ICPT) technology (Pantic *et al*., 2011; Tang *et al*., 2011; Li *et al*., 2012) which can realize the power transmission in short distance by means of the electromagnetic (Budhia *et al*., 2011; Kazimierczuk, 2009) coupling between primary and secondary coils. Compared with the conventional electric-wire mode, the wireless mode for battery charging is without contact sparks, carbon deposits and uncovered electric-wire being exposed to the environments, which make this charging mode itself have advantages of good safety and flexibility, high reliability, low maintenance. Therefore, the novel contactless battery charging method has obtained extensive attention from the international research institutions and related enterprises (Madawala and Thrimawithana, 2011; Lorico *et al*., 2011).

At present, two kinds of battery charging modes commonly used in practice are constant-voltage mode and constant-current mode. In the constant-voltage charging mode, the charge current that descends on uncertain changing rate will make its value too large in the initial stage and too small in the end stage. The low charge current in constant-voltage mode will lead to the shortage of charge, extending the charge time, reducing the battery's working life (Panasonic, 1998). While the constant-current mode can overcome the charging disadvantages mentioned in the constant-voltage mode and not only ensure that battery is fully charged but also effectively reduce the charge time (Ikeya *et al*., 2002). However, to maintain the charge current constant, the charge voltage must be increased as the battery capacity rises. To achieve the constant-current charging mode, modeling and control for the ICPT contactless battery charging system is inevitable.

Aiming at the dynamic modeling for power electronic system, most of currently used methods are based on one assumption that the system harmonic components and their edge-frequency components can be ignored (Davoudi and Jatskevich, 2007; Oettmeier *et al*., 2009). The small-signal model established by approximate equivalent and average linearization method, only retaining the low-frequency part of the original signal, hence is suitable for describing the nonlinear dynamic behavior with slow time-varying characteristic (Galigekere and Kazimierczuk, 2011). However, the additional resonant network used to create the zero-voltage or zero-current switching condition for ICPT contactless charging system makes some circuit variables showing rapidly oscillating characteristic, which causes the small-signal modeling methods inapplicable and limited. In order to analyze the complex dynamic behavior of ICPT contactless battery charging system, a

Corresponding Author: Yan-Ling Li, Department of Electrical Engineering, Southwest Jiaotong University, China

generalized state-space averaging method (Dong *et al*., 2008; Rimmalapudi *et al*., 2007) based on the frequency-domain decomposition is introduced, which can describe not only the DC variables with slow time-varying characteristics but also the AC variables with rapidly oscillating characteristics.

In the practical application of ICPT technology, control algorithms independent of the object models are commonly used. They are relatively simple and easy to be implemented, also have certain robustness to the interference signals and dynamic perturbations in system's operating process. However, the system's overshoot, stability, reliability and other performance indexes have been ignored in the design of control algorithms (Madawala and Thrimawithana, 2012; Sun *et al*., 2011), so the control results will not be always good to the complex ICPT system which is nonlinear, time-varying, coupling and uncertain.

Based on the object model built by generalized state-space averaging method and comprehensively considering the uncertainties of low frequency parameters and high frequency un-modeled part, a H∞ synthesis control algorithm solved by the linear matrix inequality method (Talebi, 2007; Gahinet *et al*., 2010; Pujol *et al*., 2007; Nguang *et al*., 2007) is proposed, which chooses the robust stability and robust performance as the design indexes in order to inhibit the adverse effects of interference signals and dynamic perturbations on the constant-current control for the contactless battery charging system effectively.

A CONTACTLESS BATTERY CHARGING SYSTEM BASED ON ICPT TECHNOLOGY

As shown in Fig. 1, the contactless battery charging system based on ICPT technology consists of the primary part for power supply and secondary part for power pickup which are electrically isolated from each other. Because the capability of power pickup in secondary coil depends on the power density of primary electro-magnetic field, it's necessary to convert the power supply from DC form to high-frequency AC form by alternately switching the pairs (S_1 S_4 and S_2' S_3) of a full-bridge inverter network. In order to reduce the switching power losses, the voltage and current stress and EMI, the direction of charging current into the resonant circuit should be alternated on the condition of zero-current crossing. The power picked-up by secondary coil is transformed from AC form to DC form through a full-bridge rectifier consisting of 4 diodes and then filtered by L_f and C_f to charge the battery directly.

If the mutual inductance between the primary and secondary coils is M, according to electromagnetic induction principle, the electromotive force induced in secondary coil that is the so called open-circuit voltage can be defined by:

$$V_{OC} = \omega M I_{Lp} \tag{1}$$

Accordingly, the formula for calculating the short-circuit current on secondary side is:

$$I_{SC} = \frac{M}{L_s} I_{Lp} \tag{2}$$

For the secondary resonant circuit with the parallel structure, the mathematical relation between the resonant voltage V_{Cs} and the open-circuit voltage V_{OC} can be described as:

$$V_{Cs} = Q_s V_{OC} \tag{3}$$

where, Q_s is the quality factor of secondary resonant circuit and equal to:

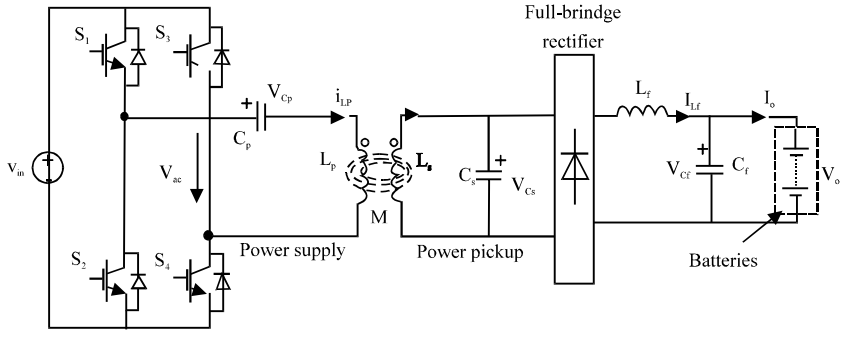

Fig. 1: Circuit topology for the contactless battery charging system

$$Q_s = \frac{R_{ac}}{\omega L_s} \tag{4}$$

where, R_{ac} is the effective AC load for reflecting the full DC load after the rectifier.

Therefore, the maximum transferred power for the contactless battery charging system can be calculated by:

$$P_{o,max} = V_{Cs} I_{SC} = \omega \frac{M^2}{L_s} I_{Lp}{}^2 Q_s \tag{5}$$

According to, the maximum possible pickup power in secondary coil can be increased by the best possible pickup design especially the electro-magnetic mechanism, which ensures that M^2/L_s ratio is optimum within any given design constrains, so the high permeability of magnetic material is preferable for high power transmission. High frequency of operation can be benefit to promote the power pickup but it is limited by switching losses and ratings of high-power semiconductor switches. The operation at high values of Q_s will also increase the power pickup but it is usually considered to be undesirable due to practical reasons such as instability and susceptibility to component tolerances. To generate high track current, primary power supply must essentially be operated at a high voltage within the ratings of high-power semiconductor devices, which can be simply adjusted by a DC/DC converter.

GENERALIZED STATE-SPACE AVERAGING MODEL

There are not only DC variables with slow time-varying characteristics but also AC variables with rapidly oscillating characteristics, so it's first to establish the generalized state-space averaging model for the contactless battery charging system based on ICPT technology.

According to Kirchhoff's law, the differential equations in time-domain for ICPT contactless battery charging system with a DC voltage source input are expressed as:

$$\begin{cases} L_p i_{Lp}'(t) + R_{Lp} i_{Lp}(t) + v_{Cp}(t) - M i_{Ls}'(t) = f_p(t) v_{in} \\ L_s i_{Ls}'(t) + R_{Ls} i_{Ls}(t) + v_{Cs} = M i_{Lp}'(t) \\ C_p v_{Cp}'(t) = i_{Lp}(t) \\ C_s v_{Cs}'(t) + f_s(t) i_{Lf}(t) = i_{Ls}(t) \\ L_f i_{Lf}'(t) + R_{Lf} i_{Lf} + v_{Cf} = f_s(t) v_{Cs}(t) \\ C_f v_{Cf}'(t) + \dfrac{v_{Cf}(t) - v_o}{R_m} = i_{Lf}(t) \end{cases} \tag{6}$$

where, R_{Lp}, R_{Ls} and R_{lf}, respectively represent the internal resistances of inductors L_p, L_s and L_f and R_m is a small resistor in series with the battery for detecting the value of charge current indirectly.

In Eq. 7 and 8, $f_p(t)$ and $f_s(t)$ are, respectively used to describe the direction of energy flows in primary inverter and secondary rectifier. They can be defined in binary logic form as:

$$f_p(t) = \begin{cases} 1 & mT < t < (2m+1)T/2, m \in I \\ -1 & (2m+1)T/2 < t < (m+1)T, m \in I \end{cases} \tag{7}$$

$$f_s(t) = \begin{cases} 1, & mT + \dfrac{\theta T}{2\pi} < t < mT + \dfrac{(\pi+\theta)T}{2\pi}, m \in I \\ -1, & mT + \dfrac{(\pi+\theta)T}{2\pi} < t < (m+1)T + \dfrac{\theta T}{2\pi}, m \in I \end{cases} \tag{8}$$

The form of $f_s(t)$ is similar to that of $f_p(t)$ but in order to model the contactless battery system, it will be very essential to determine the phase-error. Through the Norton equivalent circuit analysis, it's found that the output current i_{Lp} and the input voltage v_{Cs} have the same phase, namely:

$$f_s(t) = f_p(t) \tag{9}$$

Due to AC variable with small waveform distortion under the condition of system operating around the nominal frequency and DC variable with small fluctuation through the effective filtering, the reasonable approximation can be obtained by considering the low-order Fourier series of circuit variables and further simplification is possible by omitting odd harmonics of DC variable and even harmonics of AC variable. Therefore, we can choose the first-order and third-order harmonic components to approximate AC variable; while only choose the zero-order harmonic component to approximate DC variable, as the following forms:

$$\begin{aligned} &i_{Lp}(t) = \sum_{k=\pm1,\pm3} \langle i_{Lp} \rangle_k e^{jk\omega t}, v_{Cp}(t) = \sum_{k=\pm1,\pm3} \langle v_{Cp} \rangle_k e^{jk\omega t} \\ &i_{Ls}(t) = \sum_{k=\pm1,\pm3} \langle i_{Ls} \rangle_k e^{jk\omega t}, v_{Cs}(t) = \sum_{k=\pm1,\pm3} \langle v_{Cs} \rangle_k e^{jk\omega t} \\ &i_{Lf}(t) = \langle i_{Lf} \rangle_0, v_{Cf}(t) = \langle v_{Cf} \rangle_0 \end{aligned} \tag{10}$$

where, represents the k-order Fourier coefficient of the circuit variable, namely the amplitude of relevant harmonic component.

Moreover, the odd harmonic components of AC variable are conjugate and symmetric, namely:

$$\langle \cdot \rangle_k = \langle \cdot \rangle_{-k}^{*} = \mathrm{Re}\langle \cdot \rangle_k + j\mathrm{Im}\langle \cdot \rangle_k \tag{11}$$

Thus, if the real and imaginary parts of the odd harmonic components or in frequency-domain can be solved respectively, then according to equation we can

also obtain their relevant AC variable in time-domain. It is the reason why the harmonic components are taken as the generalized state-space variables, namely:

$$\begin{aligned}\mathbf{x}(t)=[&\mathrm{Re}\langle i_{Lp}\rangle_1,\mathrm{Im}\langle i_{Lp}\rangle_1,\mathrm{Re}\langle i_{Lp}\rangle_3,\mathrm{Im}\langle i_{Lp}\rangle_3,\\&\mathrm{Re}\langle v_{Cp}\rangle_1,\mathrm{Im}\langle v_{Cp}\rangle_1,\mathrm{Re}\langle v_{Cp}\rangle_3,\mathrm{Im}\langle v_{Cp}\rangle_3,\\&\mathrm{Re}\langle i_{Ls}\rangle_1,\mathrm{Im}\langle i_{Ls}\rangle_1,\mathrm{Re}\langle i_{Ls}\rangle_3,\mathrm{Im}\langle i_{Ls}\rangle_3,\\&\mathrm{Re}\langle v_{Cs}\rangle_1,\mathrm{Im}\langle v_{Cs}\rangle_1,\mathrm{Re}\langle v_{Cs}\rangle_3,\mathrm{Im}\langle v_{Cs}\rangle_3,\\&\langle i_{Lf}\rangle_0,\langle u_{Cf}\rangle_0]^T\end{aligned} \tag{12}$$

Then based on the differential property of Fourier series (Oppenheim *et al*., 1996), the time-domain differential equations for ICPT contactless battery charging system can be further transformed to the frequency-domain form which takes the harmonic components as its variables, as shown in Eq. 13:

$$\begin{cases}\langle i_{Lp}\rangle_{k=1,3}' = \psi^{-1}\left(L_sR_{Lp}\langle i_{Lp}\rangle_k + L_s\langle v_{Cp}\rangle_k + MR_{Ls}\langle i_{Ls}\rangle_k + M\langle v_{Cs}\rangle_k\right)\\ \qquad -\psi^{-1}v_{in}L_s\langle f_p\rangle_k - jk\omega\langle i_{Lp}\rangle_k\\ \langle v_{Cp}\rangle_{k=1,3}' = C_p^{-1}\langle i_{Lp}\rangle_k - jk\omega\langle v_{Cp}\rangle_k\\ \langle i_{Ls}\rangle_{k=1,3}' = \psi^{-1}\left(MR_{Lp}\langle i_{Lp}\rangle_k + M\langle v_{Cp}\rangle_k + L_pR_{Ls}\langle i_{Ls}\rangle_k + L_p\langle v_{Cs}\rangle_k\right)\\ \qquad -\psi^{-1}v_{in}M\langle f_p\rangle_k - jk\omega\langle i_{Ls}\rangle_k\\ \langle v_{Cs}\rangle_{k=1,3}' = C_s^{-1}\left(\langle i_{Ls}\rangle_k - \langle f_s i_{Lf}\rangle_k\right) - jk\omega\langle v_{Cs}\rangle_k\\ \langle i_{Lf}\rangle_{k=0}' = -L_f^{-1}\left(\langle v_{Cf}\rangle_k + R_{Lf}\langle i_{Lf}\rangle_k - \langle f_s v_{Cs}\rangle_k\right) - jk\omega\langle i_{Lf}\rangle_k\\ \langle v_{Cf}\rangle_{k=0}' = C_f^{-1}R_m^{-1}\left(v_o - \langle v_{Cf}\rangle_k + R_m\langle i_{Lf}\rangle_k\right) - jk\omega\langle v_{Cf}\rangle_k\end{cases} \tag{13}$$

where, ψ is used to substitute the expressions of M^2-L_pL_s.

Further, according to the convolution property of Fourier series, the nonlinear terms with the coupled form of circuit variable and switching function in equation can be approximately equal to:

$$\langle f_s i_{Lf}\rangle_1 = \sum_{i=-3,-1,0,1,3}\langle f_s\rangle_{1-i}\langle i_{Lf}\rangle_i = \langle f_s\rangle_1\langle i_{Lf}\rangle_0 \tag{14}$$

$$\langle f_s i_{Lf}\rangle_3 = \sum_{i=-3,-1,0,1,3}\langle f_s\rangle_{3-i}\langle i_{Lf}\rangle_i = \langle f_s\rangle_3\langle i_{Lf}\rangle \tag{15}$$

$$\begin{aligned}\langle f_s v_{Cs}\rangle_0 = &\sum_{i=-3,-1,0,1,3}\langle f_s\rangle_{0-i}\langle v_{Cs}\rangle_i = \langle f_s\rangle_3\langle v_{Cs}\rangle_{-3}\\&+\langle f_s\rangle_1\langle v_{Cs}\rangle_{-1} + \langle f_s\rangle_{-1}\langle v_{Cs}\rangle_1 + \langle f_s\rangle_{-3}\langle v_{Cs}\rangle_3\end{aligned} \tag{16}$$

Substitute Eq. 4, 15 and 16 for the relevant nonlinear terms in equation and an approximate linear model can be achieved. Then, separate the real and imaginary parts of all the harmonic components and obtain a generalized state space description for ICPT contactless battery charging system, namely:

$$\dot{\mathbf{x}}(t) = A\mathbf{x}(t) + B_1v_o(t) + B_2v_{in}(t) \tag{17}$$

Choose the charge current of the battery in secondary side as the system output and then the output equality can be represented as:

$$\mathbf{y}(t) = C\mathbf{x}(t) + D_1v_o(t) + D_2v_{in}(t) \tag{18}$$

H∞SUNTHESIS CONTROLLER DESIGN

For the realization of constant-current mode of the ICPT contactless battery charging system, in order to ensure the smallest possible changes of charge current, the bounded values of battery voltage and DC input voltage, it chooses the above variables as the controlled outputs which further attach the performance functions W_1, W_2 and W_3 for composing the controlled vector $z = [z_1\ z_2\ z_3]^T$. Because the variation of battery voltage in the charging process is the main adverse factor affecting the constant-current control performance, an output feedback H_∞controller u (*s*) = K(s)e (s) will be designed for the controlled object with the battery voltage as its disturbance input in order to make the closed-loop system shown in Fig. 2 satisfying the following properties:

- It should be always internal stable, that is to say, the real parts of all system state matrix's eigenvalues are negative
- The H-infinite norm of the transfer function $T_{dz}(s)$ from the disturbance input d to controlled output should be less than 1, namely:

$$\|T_{dz}(s)\|_\infty < 1 \tag{19}$$

Determination of performance weighting functions: Comprehensively taking the high frequency un-modeled part that shows the multiplicative perturbation of $(I+\Delta_m)G$ and the uncertainty of low frequency parameters that shows the additive perturbation of $G+\mathbf{\Delta}_a$ into account, the performance functions $W_1(s)$ and $W_3(s)$ are, respectively used to describe the norm boundedness of the multiplicative and additive perturbations, namely:

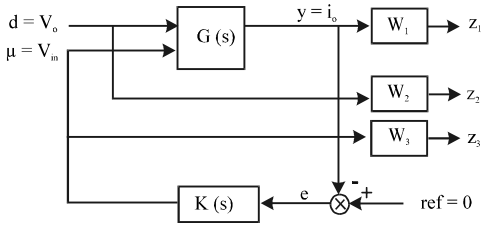

Fig. 2: Diagram of the closed-loop system

$$\|\Delta_m\|_\infty < \|W_1(j\omega)\|_\infty \tag{20}$$

$$\|\Delta_a\|_\infty < \|W_3(j\omega)\|_\infty \tag{21}$$

The function $W_2(s)$ is a low-pass filter whose bandwidth equals that of the disturbance input for representing the disturbance's spectrum characteristics. On the premise of making the system achieve the dynamic quality requirements without increase in the controller order, if the bandwidth of low-frequency disturbance is ω_L, $W_2(s)$ can be chosen as:

$$W_2(s) = \frac{k_2}{j\omega/\omega_2 + 1} \tag{22}$$

where, ω_2 should satisfy $\omega_2 = \omega_c > \omega_L$ for effectively inhibiting the low-frequency disturbance and ω_c is the desired pened-loop cutoff frequency.

For embodying the high frequency un-modeled part in control system, $W_1(s)$ should have the high-pass property and its rising rate of amplitude-frequency characteristic may be high on the condition of preserving the useful signal. Therefore, the bandwidth of $W_1(s)$ must be higher than that of closed-loop system desired, that is to say, the bandwidth ranges of $W_1(s)$ and $W_2(s)$ can't lap over each other.

After the functions $W_1(s)$ and $W_2(s)$ are determined, $W_3(s)$ can be taken as a constant to be adjusted so that there is the larger allowable range of parameter perturbation in the low frequency-domain.

Based on the above analysis, the performance weighting functions are finally determined as:

$$W_1(s) = \frac{10s^2 + 8s + 0.1}{s^2 + 1.8s + 10}$$

$$W_2(s) = \frac{0.1}{10s + 1}$$

$$W_3(s) = 0.01$$

Solving synthesis problem by LMI method: Before designing the output feedback H_∞ controller, the state space description of open-loop system with two inputs and two outputs as shown in Fig. 2 can be expressed as:

$$\begin{cases} \dot{x}(t) = Ax(t) + B_1 d(t) + B_2 u(t) \\ z(t) = C_1 x(t) + D_{11} d(t) + D_{12} u(t) \\ e(t) = C_2 x(t) + D_{21} d(t) + D_{22} u(t) \end{cases} \tag{23}$$

Assume that the state space realization of the desired controller can be expressed as:

$$\begin{aligned} \dot{\hat{x}}(t) &= A_k \hat{x}(t) + B_k e(t) \\ u(t) &= C_k \hat{x}(t) + D_k e(t) \end{aligned} \tag{24}$$

where, $\hat{x} \in R^{n_k}$ is the state variables and A_k B_k C_k D_k are the coefficient matrixes to be solved for H∞ synthesis controller.

With regard to such a continuous-time system, the LMI method is utilized to solve the H_∞ synthesis problem. First, it needs to find two symmetric positive definite matrixes X and Y such that [Eq. 17]:

$$\begin{bmatrix} N_o & 0 \\ 0 & I \end{bmatrix}^T \begin{bmatrix} A^T X + XA & XB_1 & C_1^T \\ B_1^T X & -I & D_{11}^T \\ C_1 & D_{11} & -I \end{bmatrix} \begin{bmatrix} N_o & 0 \\ 0 & I \end{bmatrix} < 0 \tag{a}$$

$$\begin{bmatrix} N_c & 0 \\ 0 & I \end{bmatrix}^T \begin{bmatrix} AY + YA^T & YC_1^T & B_1 \\ C_1 Y & -I & D_{11} \\ B_1^T & D_{11}^T & -I \end{bmatrix} \begin{bmatrix} N_c & 0 \\ 0 & I \end{bmatrix} < 0 \tag{b}$$

$$\begin{bmatrix} X & I \\ I & Y \end{bmatrix} \geq 0 \tag{C}$$

where, N_o used for evaluating the part incapable of being reflected by the measured output and N_c used for evaluating the part incapable of being affected by the control input, are the matrixes whose column vectors are respectively composed by arbitrary set of basis vectors of the kernel space of $[C_2\ D_{21}]$ and $[B_2^T\ D_{12}^T]$:

$$X\text{-}Y^{-1} = X_2 X_2^T \tag{25}$$

Then, apply the singular-value decomposition method to solve equation and obtain the matrix where can be the rank of $X\text{-}Y^{-1}$ and further construct the following matrix:

$$X_c = \begin{bmatrix} X & X_2^T \\ X_2 & I \end{bmatrix} \tag{26}$$

Lastly, by using the construction matrix to substitute for X_c in, a linear matrix inequality that is only dependent of one matrix variable formed by all the coefficient matrixes of H_∞ synthesis controller is obtained:

$$H_{X_c} + P_{X_c}^T K Q + Q^T K^T P_{X_c} < 0 \tag{27}$$

In , the matrixes H_{Xc}, P_{Xc} and Q are all known and certain and can be represented as:

$$H_{X_c} = \begin{bmatrix} A_0^T X_c + X_c A_0 & X_c B_0 & C_0^T \\ B_0^T X_c & -I & D_{11}^T \\ C_0 & D_{11} & -I \end{bmatrix} \tag{28}$$

$$P_{X_c}=\left[\bar{B}^T X_c \quad 0 \quad \bar{D}_{12}{}^T\right] \tag{29}$$

$$Q=\left[\bar{C} \quad \bar{D}_{21} \quad 0\right] \tag{30}$$

where, A_0, B_0,C_0, B, C, D_{12} and D_{21} are, respectively written as:

$$A_0=\begin{bmatrix} A & 0 \\ 0 & 0 \end{bmatrix}, {}^T B_0=\begin{bmatrix} B_1 \\ 0 \end{bmatrix}, C_0=\begin{bmatrix} C_1 & 0 \end{bmatrix}$$

$$\bar{B}=\begin{bmatrix} 0 & B_2 \\ I & 0 \end{bmatrix}, \bar{C}=\begin{bmatrix} 0 & I \\ C_2 & 0 \end{bmatrix}, \bar{D}_{12}=\begin{bmatrix} 0 & D_{12} \end{bmatrix}$$

$$\bar{D}_{21}=\begin{bmatrix} 0 \\ D_{21} \end{bmatrix}$$

So far, the H_∞ synthesis problem is transformed to the feasibility problem of a linear mat rix inequality system which is only dependent of the controller parameters to be solved. Thus, it's easy to achieve a H_∞ output feedback controller based on the LMI method.

For the closed-loop system, H-infinite norm of the transfer function $T_{dz}(s)$ is defined as upper bound of the maximum singular-value for the frequency response at each frequency ω (Chen, 2010), namely:

$$\left\|T_{dz}(s)\right\|_\infty = \sup_\omega \bar{\sigma}(T_{dz}(j\omega)) \tag{31}$$

The curves of maximum singular-value for frequency response on the range of $[10^{-4}, 10^6]$ are shown in Fig. 3. And seen from the distribution curves which are obviously under the line of 10^0, H-infinite norm of transfer function $T_{dz}(s)$ satisfies the inequality of:

$$\left\|T_{dz}(s)\right\|_\infty <1 \tag{32}$$

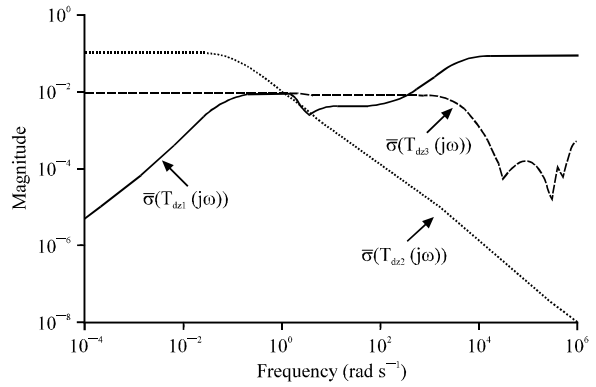

Fig. 3: Singular value plot of $T_{dz}(j\omega)$

Therefore, the H_∞ synthesis control system designed by LMI method has achieved the predetermined performance index. Moreover, its internal stability has also been verified by solving all the poles of the closed-loop transfer function.

SIMULATION AND EXPERIMENTAL RESULTS

On the basis of circuit parameters shown in Table 1, the state matrixes for the open-loop system are obtained and further a H_∞synthesis control algorithm is designed by the LMI method. With the help of the proposed H_∞ synthesis algorithm, the robust stability and performance of operating at the constant-current charging mode for the contactless battery charging system is first verified via Matlab/ Simulink simulation and then realized and tested in the laboratory.

Simulation results: The simulation model is established on the Matlab/ Simulink platform according to the control diagram for contactless battery charging system in Fig. 1. In the practical application, the maximum current allowed by the battery is commonly used in the constant-current charging mode in order to reduce the charge time effectively. However, the high charge current at the latter stage can not only make some energy be wasted on the form of electrolyte heating but also decrease the battery's capacity and cycle life. Consequently, it's essential to dynamically regulate the charge current and make it equal to a proper value according to the actual battery state at the different charging stage which is benefit for decreasing the electrolyte heat production, increasing the charge efficiency and extending the battery's cycle life.

For simulating the process of constant-current control at the different stage, the total simulation time is set as 20 sec and the reference value for constant-current charging equals 2A, 3A and 2A on the time interval of 0~10s, 10~15s and 15~20s, respectively. The transient response of the closed-loop system with the help of H_∞synthesis control is shown in Fig. 4.

Table 1: Circuit parameters

Parameters	Values
Inductance L_p (μH)	154
Capacitance C_p (μF)	0.47
Equivalent resistance R_{ip} of inductance L_p (Ω)	0.185
Mutual inductance M (μH)	43.7
Secondary resonant capacitance C_s (μF)	1
Secondary resonant inductance L_s (μH)	60
Equivalent resistance R_{is} of inductance L_s (Ω)	0.087
Filter inductance L_i (Ω)	4.8
Filter capacitance C_i (μF)	220
Measurement resistance R_m (Ω)	0.5
Nominal voltage Of charging battery (V)	3.7
Rated capacity of charging battery (Ah)	3.2

Figure 4 shows the transient response of tracking the current reference. It can be seen that although the reference of charge current is changed, the H_∞ synthesis system can still track the changed reference for charging the battery. It takes about 2 seconds and has a small overshoot for reaching another steady state. Therefore, the proposed H_∞ synthesis algorithm can achieve the constant-current control at the different stage of actual battery demand.

As the main adverse factor affecting the constant-current control performance, the variation of battery voltage in the charging process is simulated by a rising staircase signal. In the simulation process, predetermine the value of battery voltage at the time intervals of 5~10s, 10~15s, 15~20s is respectively equal to 3V, 3.5V and 4V, while keep the reference of charge current be equal to 2A at all times. The transient response for inhibiting the adverse effects of battery voltage changes on the system is shown in Fig. 5.

As can be seen from Fig. 5, H8 synthesis system can effectively restrain the effect of battery voltage variations on the charge current and rapidly recover its steady-state of 2A by regulating the input DC voltage of the controlled object, but the charge current in the transient response process has an inverse sharp peaked value. The simulation results show that the H_∞ synthesis system has certain robustness to the battery voltage variations by resisting its effect on the system stability and performance rapidly and effectively.

Experimental results: In the practical experiment, considering that the input of H_∞ synthesis controller is the discrete sample signal feedback from the secondary side, it's necessary to discrete the continuous H_∞ control algorithm to fulfill the function of digital signal processing. The discrete similar method in frequency-domain based on zero-order holder is used to obtain the pulse transfer function of H_∞ controller and then the pulse transfer function is further transformed to a difference equation as described in equality of:

$$y_k = \sum_{i=1}^{n} a_i y_{k-i} + \sum_{j=0}^{m} b_j u_{k-j}, m=n=20 \quad (33)$$

where, y_k is the control signal at the current moment of k and y_{k-i} and u_{k-j}, respectively represent the control signal and the sample signal at the moment of k-i and k-j, while a_i (i = 1,…,20)and b_j (j = 0,…,20) are corresponding coefficients for the terms of y_{k-i} and u_{k-j}, taking values as:

$[a_1,\cdots,a_{20}]$=[2.05,-1.10,0.0532,-2.62e-10,9.68e-19, -1.35e-32, 5.35e-46,1.88e-59,8.59e-76,-4.86e-92,5.73e-109,1.46e-126, -4.32e-143, 1.40e-160,7.03e-179,-4.08e-196,-2.05e-214, -3.42e-233,-1.14e-251,-1.66e-270]

$[b_0,\cdots,b_{20}]$=[0,13.0,-25.7,12.6,0.0749,-3.69e-10, 1.36e-18, -3.83e-32,1.36e-45,5.13e-60, 2.11e-75,-4.15e-92,8.81e-110, 3.54e-127, 9.73e-145,-4.44e-162,2.93e-181,1.14e-198, -2.81e-217,-3.16e-236,7.13e-256]

Figure 6 shows the experimental implementation for the H∞ synthesis control system.

Because the battery's internal resistance will change in the charging process, a resistor R_m is connected in series with battery in order to detect the value of charge current precisely based on the equality of $i_o = v_m/R_m$. For transmitting the sample voltage v_m from the secondary side to the primary side without any medium continuity, a practical MCU transmission system integrating the nRF24L01 transceiver chips is also designed for achieving the wireless communication between the primary and secondary sides. Considering that the fast sampling and real time processing functions of H_∞ controller are required to achieve good control results, the control module realized on a DSP development platform with the main chip of TMS320F2812, on one hand, is used to achieve the discrete control algorithm for calculating the control variable and on the other hand, is also used to generate

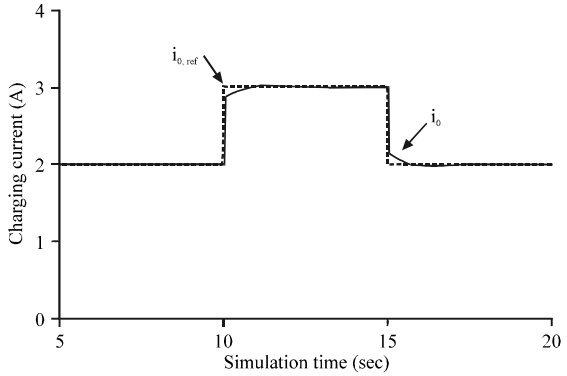

Fig. 4: Transient response to the reference of charging current

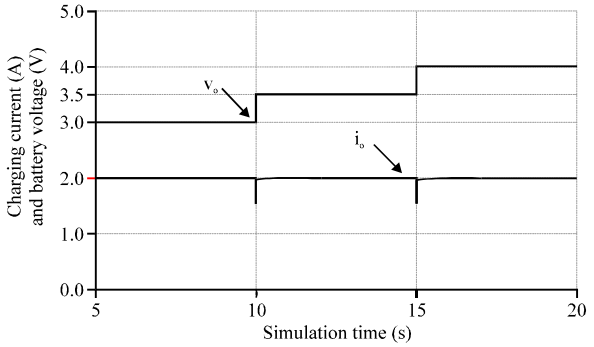

Fig. 5: Transient response to the changed battery voltage

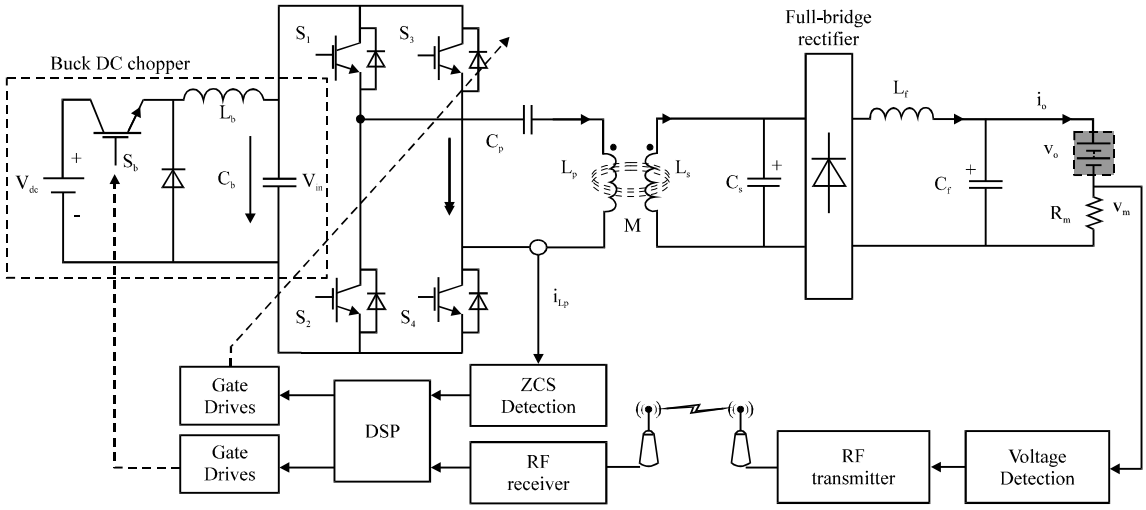

Fig. 6: Experimental implementation diagram

gate drives for soft-switching the devices of high- frequency inverter by detecting the zero crossing points and the cases of in positive or negative direction of the current i_{Lp}. Moreover, there is a DC/DC converter added on the primary side to indirectly regulate the input voltage of high-frequency inverter in the practical experiment. Accordingly, the control variable of the closed-loop system is changed to the gate drive of S_b.

The practical experiment is carried out on the initial condition that the input voltage of DC/DC converter and the gate drive frequency for S_b are respectively set at 21V and 80KHz. The experimental results in start-up process with the charge current reference of 2A are shown in Fig. 7.

Figure 7 includes the transient responses of the detection voltage v_m and resonant current i_{Lp} in start-up process. It should be noted that the value of 2A for charge current is equivalent to the value of 1V for detection voltage when R_m is equal to 0.5Ω. It can be seen that after power-up for the system, the H_∞ controller rapidly acts to regulate the detection voltage by controlling the input voltage of high-frequency inverter and about 50 msec is taken to reach the steady state of 1V with an overshoot of 10% during the transient response process. At the steady state, the detection voltage can well approach its equivalent reference with a very small static error between them. The results indicate that the H∞ control system has realized the constant-current charging mode with good dynamic response characteristics.

For the contactless battery charging system based on Inductively Coupled Power Transfer (ICPT) technology, the perturbations of low frequency parameters especially small change in load, will be inevitably introduced into the

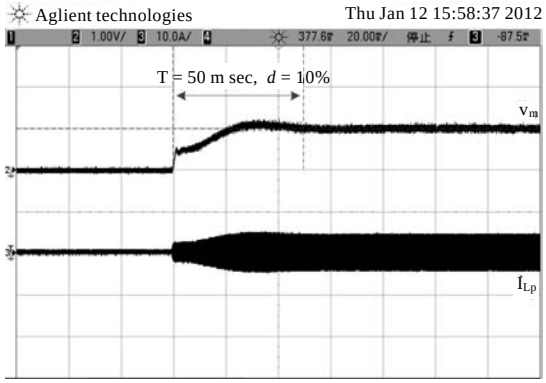

Fig. 7: Transient response in start-up process

system and cause many issues for the normal operation, such as decrease in transmission power and distance, sine-wave distortion, EMC interference, system detuning, performance deterioration, working deviated from the design requirements and even system instability. In the actual experiment, a resistor of 5.1Ω is connected in parallel with the charge circuit branch on secondary side and at the same time an option switch is used to implement the switching in or switching out for this resistor, so that the robust stability and robust performance of H_∞ synthesis control system with load variations can be analyzed.

Figure 8 shows the transient response of the closed loop system in load changing process. Load condition I represents the situation of switching out for the attached resistor, namely the initial circuit state, while load condition II represents the situation of switching in for

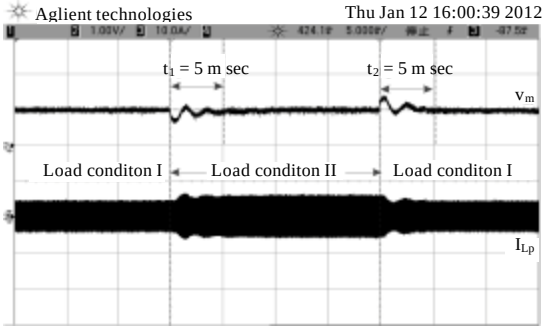

Fig. 8: Transient response to load changing

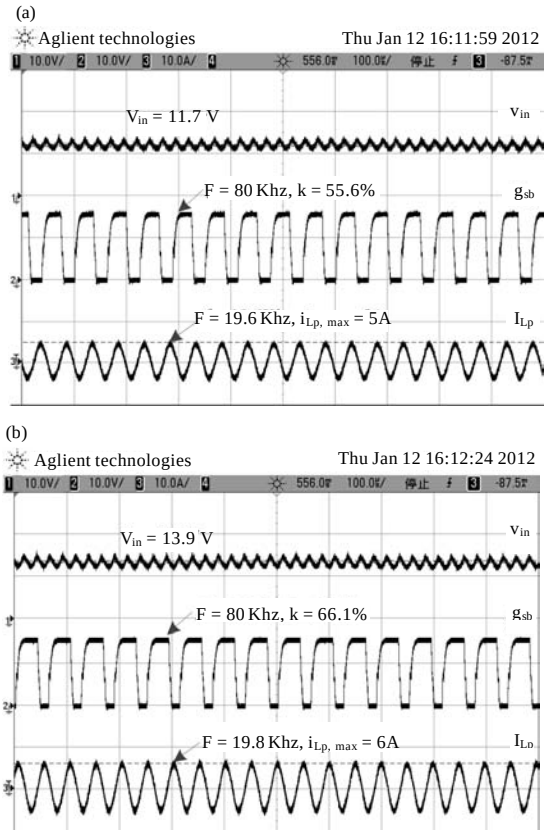

Fig. 9(a-b): Steady-states under the different load conditions. (a) Load condition I and (b) Load condition II

the attached resistor, namely the attached resistor in parallel with the charge circuit branch. When load is changed, the transient process just costs about 5ms to effectively reduce and eliminate the impact of load variations on the controlled variable in spite of certain overshoot, which indicates H_∞ synthesis control system not only has robust stability but also satisfy some robust performance to the load variations.

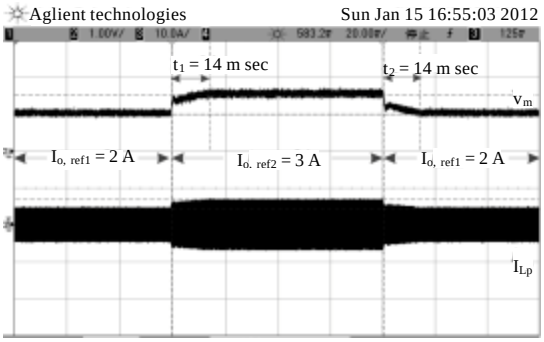

Fig. 10: Transient response for tracking reference value

The steady-state waveforms under the different load conditions are shown in Fig. 9, including the gate drive signal of DC/DC converter, input voltage of high-frequency inverter and primary resonant current. As noted, V_{in} represents the average value of DC input voltage v_{in}.

Compared the experimental results with each other, it can be concluded that with the load changed from condition I to condition II, the duty cycle in one switching period of DC/DC converter is changed from 55.6% to 66.1%, while the average value of input voltage of high-frequency inverter is increased from 11.7V to 13.9V and the amplitude of primary resonant current as well as the soft-switching frequency is also increased with the load variations, but still has good sinusoidal oscillation characteristic. Consequently, it's evident that although the operation condition is changed due to the load perturbations, H_∞ synthesis control system can always achieve the constant-current charging mode by adjusting the input voltage of high-frequency inverter.

Lastly, the transient response to different reference values of charge current is shown in Fig. 10.

Figure 10: Transient response for tracking reference value Seen from Fig.10, the steady-state values of detection voltage are respectively equal to 1V and 1.5V in the cases of $i_{o,ref1}$=2A and $i_{o,ref1}$= 3A, so it is illuminated that H_∞ synthesis control system can track the reference values of charge current at the different stage of actual battery demand. And because the transient response process only costs about 14 msec accompanying with hardly any overshoot, the experiment results also indicates that the system has good dynamic tracking performance with the help of H_∞ synthesis controller.

CONCLUSION

Modeling for ICPT contactless battery charging system with the oscillating and nonlinear characteristics is achieved by the generalized state-space averaging method in view of the factorization for low-order Fourier series in frequency-domain. And then the performance weighting functions are attached in the GSSA model for reflecting the uncertainties of low frequency parameters and the high frequency un-modeled part in order to improve the mathematical model for well describing the system's dynamic behaviors.

To fulfill a robust stability and robust performance design for ICPT contactless battery charging system, the H_∞ synthesis control problem is transformed to the feasibility problem of a linear matrix inequality system which is only dependent of the controller parameters to be solved and then a H_∞ synthesis control algorithm is proposed by solving the linear matrix inequality system. Further the validity and feasibility of this H_∞ synthesis control system is tested and verified by the computer simulation and practical experiment.

ACKNOWLEDGMENTS

This work was supported in part by the State Key Program of National Natural Science of China (Grant No. U1234203) and the National Natural Science Foundation of China (Grant No: 51277192). The authors would like to thank all reviewers for their valuable comments.

REFERENCE

Budhia, M., G.A. Covic and G.T. Boys, 2011. Design and optimization of circular magnetic structures for lumped inductive power transfer systems. IEEE Trans. Power Electron., 26: 3096-3108.

Chen, B.M., 2010. Robust and H-Infinity Control. Springer, Berlin, Germany, ISBN-13: 9781849968584, Pages: 452.

Davoudi, A. and J. Jatskevich, 2007. Parasitics realization in state-space average-value modeling of PWM DC-DC converters using an equal area method. IEEE Trans. Circuits Syst. I: Regul. Pap., 54: 1960-1967.

Dong, L., H. Ma and F. Xu, 2008. Modeling and analysis of PWM converters with a new GSSA method. Proceedings of the 34th Annual Conference of the IEEE Industrial Electronics Society, November 10-13, 2008, Orlando, FL., USA., pp: 821-826.

Gahinet, P., A. Nemirovski, A.J. Laub and M. Chilali, 2010. LMI control toolbox for use with MATLAB®. The MathWorks Inc., Natick, MA., USA. http://saba.kntu.ac.ir/eecd/ecourses/robust/lmi.pdf.

Galigekere, V.P. and M.K. Kazimierczuk, 2011. Small-signal modeling of PWM Z-source converter by circuit-averaging technique. Proceedings of IEEE International Symposium on Circuits and Systems, May 15-18, 2011, Rio de Janeiro, Brazil, pp: 1600-1603.

Ikeya, T., N. Sawada, J. Murakami, K. Kobayashi and M. Hattori *et al*., 2002. Multi-step constant-current charging method for an electric vehicle nickel/metal hydride battery with high-energy efficiency and long cycle life. J. Power Sources, 105: 6-12.

Kazimierczuk, M.K., 2009. High-Frequency Magnetic Components. John Wiley and Sons, Natick, MA., USA., ISBN-13: 9780470748039, Pages: 496.

Li, H.L., A.P. Hu and G.A. Covic, 2012. A direct AC-AC converter for inductive power-transfer systems. IEEE Trans. Power Electron., 27: 661-668.

Lorico, A., J. Taiber and T. Yanni, 2011. Inductive Power Transfer System Integration for Battery-Electric Vehicles. In: Sustainable Automotive Technologies 2011, Hung, S., A. Subic and J. Wellnitz (Eds.). Springer, Berlin, Germany, ISBN-13: 9783642190520, pp: 75-85.

Madawala, U.K. and D.J. Thrimawithana, 2011. A bidirectional inductive power interface for electric vehicles in V2G systems. IEEE Trans. Ind. Electron., 58: 4789-4796.

Madawala, U.K. and D.J. Thrimawithana, 2012. New technique for inductive power transfer using a single controller. IET Power Electron., 5: 248-256.

Nguang, S.K., W. Assawinchaichote and P. Shi, 2007. Robust H1 control design for fuzzy singularly perturbed systems with Markovian jumps: An LMI approach. IET Control Theory Appl., 1: 893-908.

Oettmeier, F.M., J. Neely, S. Pekarek, R. DeCarlo and K. Uthaichana, 2009. MPC of switching in a boost converter using a hybrid state model with a sliding mode observer. IEEE Trans. Ind. Electron., 56: 3453-3466.

Oppenheim, A.V., A.S. Willsky and S. Hamid, 1996. Signals and Systems. 2nd Edn., Prentice Hall, New Jersey, USA., ISBN-13: 978-0138147570, Pages: 957.

Panasonic, 1998. Sealed lead acid handbook: Charging methods. http://www.commutercars.com/downloads/PanasonicSLAHandbook.pdf

Pantic, Z., S. Bai and S.M. Lukic, 2011. ZCS LCC-compensated resonant inverter for inductive-power-transfer application. IEEE Trans. Ind. Electron., 58: 3500-3510.

Pujol, G., J. Rodellar, J.M. Rossell and F. Pozo, 2007. Decentralised reliable guaranteed cost control of uncertain systems: An LMI design. IET Control Theory Appl., 1: 779-785.

Rimmalapudi, S.R., S.S. Williamson and A. Nasiri, 2007. Validation of generalized state space averaging method for modeling and simulation of power electronic converters for renewable energy systems. J. Electr. Eng. Technol., 2: 231-240.

Sun, Y., C.S. Tang, A.P. Hu, H.L. Li and S.K. Nguang, 2011. Multiple soft-switching operating points-based power flow control of contactless power transfer systems. IET Power Electron., 4: 725-731.

Talebi, H.A., 2007. Lecture notes on robust control. Department of Electrical Engineering, Tehran Polytechnic, Iran.

Tang, C.S., Y. Sun, X. Dai, Z.H. Wang, Y.G. Su and A.G. Hu, 2011. Analysis of multiple resonant operating points and their autonomous oscillation stabilities in inductive power transfer systems. Acta Physica Sinica, 60: 738-746.